Available online at www.sciencedirect.com

SciVerse ScienceDirect

Ceramics International 39 (2013) 6657–6667

CERAMICS INTERNATIONAL

www.elsevier.com/locate/ceramint

Processing of different alumina–zirconia composites by slip casting

Heidy L. Calambás Pulgarin, Liliana B. Garrido, María P. Albano*

Centro de Tecnología de Recursos Minerales y Cerámica (CETMIC), C.C. 49 (B1897ZCA) M. B. Gonnet, Provincia de Buenos Aires, Argentina

Received 16 November 2012; accepted 29 January 2013
Available online 8 February 2013

Abstract

Two Al_2O_3–ZrO_2 mixture preparation routes: classical powder mixing and addition of a Zr (IV) precursor solution to a well dispersed Al_2O_3 suspension, were used to produce alumina (Al_2O_3)–zirconia (ZrO_2) slip cast composites. For the conventional powder mixing route, two commercial 3 mol% yttria-partially stabilized zirconia powders, 0.3 wt% Al_2O_3-doped (Al-doped Y-PSZ) and without Al_2O_3 (Y-PSZ), were employed. The influence of the zirconia content and the solid loading on the rheological properties of concentrated aqueous Al_2O_3–ZrO_2 slips were investigated. The density of green samples was studied and related to the degree of slip dispersion. In addition, the influence of the processing conditions on the density and microstructure development of sintered samples were investigated. By using the Zr (IV) precursor route, nano-sized ZrO_2 (ZN) particles homogeneously distributed on the Al_2O_3 particle surfaces were obtained; however, it let to aggregates of some Al_2O_3 particles with very fine ZrO_2 uniformly distributed. The viscosity and yield stress values of Al_2O_3–ZN suspensions were markedly higher than those of Al_2O_3–Al-doped Y-PSZ and Al_2O_3–Y-PSZ ones, for all the compositions and solid loading studied and resulted in a less dense packing of cast samples. However, for the composite with 10.5 vol% ZN a high sintered density and a smaller ZrO_2 grain size distribution compared with the conventional powder mixing route could be obtained.

Keywords: A. Slip casting; A. Sintering behavior; Al_2O_3–ZrO_2 suspensions; Rheological properties

1. Introduction

Recently, zirconia-toughened-alumina ceramics have received considerable attention due to their attractive properties, including high-temperature mechanical strength, good thermal shock resistance, wear and oxidation resistance, low thermal conductivity, and the close match between their thermal expansion coefficients and those of metals [1,2]. These properties make zirconia–alumina ceramics suitable for a variety of high demanding applications including dental screws, cutting blades, electrosurgical insulators, valve seals, body armor, pump components, oxygen sensors, dies, and prosthesis components such as hip joints [3,4]. The zirconia grains embedded in an alumina matrix enhance the flexural strength, fracture toughness, and fatigue resistance [5]. The toughening mechanisms identified in zirconia-reinforced alumina ceramics is attributed to the stress induced phase transformation of metastable tetragonal grains towards the monoclinic symmetry ahead of a propagating crack, leading to an increase in the work of fracture [5]. This phenomenon of transformation toughening relies on the volume expansion, 3–5%, and shear strain $\approx 7\%$ develops when tetragonal zirconia transforms to the monoclinic form [6]. Besides, microcracks extending in the stress field of a propagating crack can absorb the fracture energy, increasing the material toughness by the microcrack toughening mechanism [2]. However, studies on the application of these materials in humid environment at low temperature have shown that the tetragonal→monoclinic transformation can also be induced at the surface of ZrO_2 grains, leading to the so-called hydrothermal transformation [3] which produces a slow degradation of the composite mechanical properties. In order to reduce the ZrO_2 susceptibility to the hydrothermal instability, 3 mol% yttria-partially stabilized zirconia powder doped with 0.3 wt% Al_2O_3 can be used [6].

Colloidal shaping methods enable to achieve high microstructural homogeneity in green and sintered parts, and offer

*Corresponding author. Tel.: +54 221 4840247; fax: +54 221 4710075.
E-mail address: palbano@cetmic.unlp.edu.ar (M.P. Albano).

0272-8842/$ - see front matter © 2013 Elsevier Ltd and Techna Group S.r.l. All rights reserved.
http://dx.doi.org/10.1016/j.ceramint.2013.01.103

near-net-shaping capabilities that reduce the postsintering machining operations and the production costs [2]. The first step in the colloidal process, is the preparation of stable concentrated aqueous suspensions of the ceramic powders. At high solids loading, relatively low slip viscosity can only be achieved in the presence of an optimum dispersion state of particles. Anionic polyelectrolytes such as ammonium polyacrylate (NH_4PA) are commonly used as dispersant of ceramic powders in aqueous media [7]. The polyelectrolyte adsorbs at the solid–liquid interface and infers repulsive forces between the particles which keeps them well dispersed; the repulsive interactions are caused by electrostatic and steric effects [8].

Al_2O_3–ZrO_2 mixtures can be prepared by two routes: classical powder mixing and addition of a Zr (IV) precursor to a well dispersed Al_2O_3 suspension. In this work, these two mixture preparation routes were used to produce concentrated aqueous Al_2O_3–ZrO_2 suspensions for slip casting. For the conventional powder mixing route, two commercial 3 mol% yttria-partially stabilized zirconia powders, 0.3 wt% Al_2O_3-doped (Al-doped Y-PSZ) and without Al_2O_3 (Y-PSZ), were employed. The different textural characteristics and interfacial charge properties of the two sub micron zirconia powders were believed to strongly affect the dispersion properties of Al_2O_3–ZrO_2 suspensions. By using the Zr (IV) precursor route, it should be possible to obtain nano-sized ZrO_2 particles homogeneously distributed on the Al_2O_3 particle surfaces. The small size of the zirconia grains would retain a large amount of tetragonal zirconia in the alumina matrix after sintering with the ability to transform under applied stress; thus, contributing to the transformation toughening mechanism operating in these composites. Besides, this route may avoid the need for any stabilizing oxide due to the fact that the ZrO_2 grains can be kept below the critical size for spontaneous transformation and above the critical size needed for transformation during crack growth [6].

In this study, a series of Al_2O_3–ZrO_2 formulations were prepared either by conventional powder mixing or a colloidal method. The influence of the zirconia content and the solid loading on the rheological properties of concentrated aqueous Al_2O_3–ZrO_2 slips were investigated. The density of green samples of the different Al_2O_3–ZrO_2 composites were compared and related to the degree of slip dispersion. In addition, the influence of the processing conditions on the density and microstructure development of sintered samples were investigated.

Table 1
Compositions used for the preparation of Al_2O_3–ZrO_2 composites.

Sample[a]	Al_2O_3 (vol%)	Al-doped Y-PSZ (vol%)	Y-PSZ (vol%)	ZN (vol%)
10.5Al-doped Y-PSZ	89.5	10.5	–	
10.5Y-PSZ	89.5	–	10.5	
10.5ZN	89.5			10.5
22Al-doped Y-PSZ	78	22	–	
22Y-PSZ	78	–	22	
22ZN	78			22
50Al-doped Y-PSZ	50	50	–	
50Y-PSZ	50	–	50	

[a]The numbers 10.5, 22 and 50 in the sample codes indicate the vol% of zirconia in the composite.

2. Experimental procedure

2.1. Raw materials and powder processing

Alumina (A16 SG, Alcoa Chemicals, USA, $d_{50}=0.40$ μm), 3 mol% yttria-partially stabilized zirconia with 0.3 wt% Al_2O_3 (Saint-Gobain ZirPro, CY3Z-MA, Chine, $d_{50}=0.23$ μm) and without Al_2O_3 (Saint-Gobain ZirPro, CY3Z-NS, Chine, $d_{50}=0.64$ μm) powders were used in this study. For the colloidal method, zirconium (IV)-propoxide solution (70 wt% in 1-propanol) (Sigma–Aldrich, Ireland) was added dropwise to a stable alumina (A16) suspension in absolute ethanol. The pH was adjusted by additions of glacial acetic acid. After drying under magnetic stirring at 60 °C, the powders were thermally treated at 850 °C for 2 h in order to remove organic residuals and were subsequently attrition milled, as a suspension in alcohol, with 3 mm alumina balls for 5 h. The powders were dried and sieved to less than 45 μm. The compositions used to prepare Al_2O_3–ZrO_2 composites are summarized in Table 1. The numbers 10.5, 22 and 50 in the sample codes indicate the volume percent of zirconia in the composite.

A commercial ammonium polyacrylate solution (Duramax D 3500, Rohm & Haas, Philadelphia PA) was used as deflocculant. 35 vol% aqueous Al_2O_3–ZrO_2 suspensions with the different compositions (Table 1) and various amounts of deflocculant were prepared by suspending particles in deionized water via 40 min of ultrasound; the pH was manually adjusted to be maintained at 9 with ammonia (25%). In addition, slips with the optimum NH_4PA concentration and different solid contents were prepared at pH 9 to study the influence of the solid loading on the rheological properties.

Slips were cast in plaster molds into disks of diameter 2.61 cm. The consolidated disks were dried slowly in air for 24 h at room temperature and 24 h at 100 °C. The green samples were sintered at a heating rate of 5 °C/min up to 1600 °C with a 2-h holding time at this temperature.

2.2. Characterization techniques

The specific surface area (S_g) and the particle size distribution of the powders were measured using a Micromeritics Accusorb and a Sedigraph (Micromeritics), respectively. The morphological features of the powders were examined by scanning electron microscopy (SEM) (JEOL, JSM-6360).

To determinate the isoelectric point (IEP) of the powders, zeta potential measurements were carried out with an instrument Zetasizer nano ZS (Malvern Instruments, UK). Eight zeta potential measurements were done by the

equipment for each pH, then an average zeta potential value was automatically calculated. The pH was measured with a pH meter calibrated with buffer solutions (pH 4, 7 and 10, Merck, Germany). Zeta potential against pH curves were determined for 0.05 vol% slips of different powders: Al_2O_3, Y-PSZ, Al-doped Y-PSZ, 10.5ZN and 22ZN in the pH range of 3–10. The pH adjustment was achieved with HCl or KOH solutions. Each curve was repeated three times. The dispersion of Al_2O_3, Y-PSZ, Al-doped Y-PSZ, 10.5ZN and 22ZN powders at different pH values was studied by measuring the mean particle diameter of 2 vol% suspensions as a function of pH.

In order to determine the amount of NH_4PA adsorbed, different 35 vol% slips with the optimum NH_4PA concentration were centrifuged for 30 min at 2500 rpm and washed twice with distilled water. Then, the solid was dried at 100 °C for 24 h and analyzed by thermal gravimetric analysis (TGA) (Model STA 409, Netzsch, Inc., Germany) at a heating rate of 10 °C/min in air. The TGA data showed a negligible water weight loss at temperatures up to 100 °C and a weight loss due to the NH_4PA decomposition in a temperature range from 300° to 600 °C. This weight loss was used to determine the amount of NH_4PA adsorbed on each sample. Although the adsorption data obtained with this technique were semiquantitative, they provided a relative measure of the amount of NH_4PA adsorbed on the samples. Zeta potential vs. pH curves were determined for 0.05 vol% slips of different powders: Al_2O_3, 22Y-PSZ, 22Al-doped Y-PSZ, 10.5ZN and 22ZN with the optimum amount of NH_4PA in the pH range 3–10.

Steady state flow curves of the different Al_2O_3–ZrO_2 slips were performed by measuring the steady shear stress value as a function of shear rate in the range of shear rates between 0.5 and 542 s^{-1}using a concentric cylinder viscometer (Haake VT550, Germany) at 25 °C. A coaxial cylinder system with two gaps (sensor system NV Haake) was used. As soon as stationary conditions were reached at each shear rate, the shear rate increased in steps up to the maximum value and then decreased. The majority of the curves did not show hysteresis area.

The slips were allowed to settle under gravity, the volume fraction of sediment was measured after 40 days; this value was used to calculate the maximum packing fraction. The density of the green compacts was determined by the Archimedes method using mercury displacement. The bulk density of the sintered samples was determined by water immersion (Standard Method ASTM C20). The sintered samples were polished with a series of diamond pastes down to 1 μm. The alumina and zirconia grain sizes were measured using SEM micrographs (JEOL, JSM-6360) of polished and thermally etched surfaces.

3. Results and discussion

3.1. Powder characterization

Fig. 1 shows a micrograph of the 22ZN powder before attrition milling. Very fine zirconia particles homogeneously distributed on some agglomerated Al_2O_3 particles were observed.

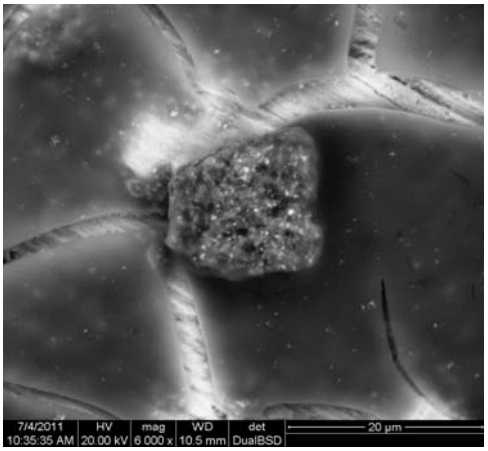

Fig. 1. SEM micrograph of the 22ZN powder before attrition milling. Al_2O_3 (the darker phase) and ZrO_2 (the brighter phase).

Fig. 2a shows the particle size distribution curves of the Al_2O_3, Y-PSZ and Al-doped Y-PSZ powders. In Fig. 2b the particle size distribution curves of the 10.5 and 22ZN powders after milling were compared with that of Al_2O_3. The particle size distribution curves of Al_2O_3 and Al-doped Y-PSZ powders were similar. Alumina showed an unimodal distribution with particle diameters > 0.1 and < 0.75 μm, the more frequent particle diameters were in the range of 0.15–0.3 μm. A slightly narrow particle size distribution was found for Al-doped Y-PSZ; thus a greater volume of finer particles (diameters between 0.10 and 0.20 μm) and a lesser volume of particles with diameters in the range of 0.20–0.55 μm were observed, the more frequent particle diameter was 0.15 μm. A bimodal distribution curve was found for Y-PSZ, the more frequent particle diameters (0.37 and 0.65 μm) were greater than those of Al_2O_3 and Al-doped Y-PSZ powders. A lesser volume of finer particles (< 0.40 μm) and a greater volume of particles with diameters in the range of 0.40–1.05 μm were observed.

A slightly wider particle size distribution was found for the ZN powders with respect to that of Al_2O_3 (Fig. 2b); a lesser volume of finer particles (< 0.35 μm) and a greater volume of particles with diameters in the range of 0.35–0.9 μm were found. The more frequent particle diameters of 10.5ZN were in the same range as those of Al_2O_3; whereas, for the 22ZN powder the more frequent particle diameters became greater (0.40–0.60 μm). Although the Zr precursor route avoided the formation of ZrO_2 aggregates on the Al_2O_3 particles (Fig. 1), it let to aggregates of some Al_2O_3 particles with very fine ZrO_2 uniformly distributed. The diameters of the Al_2O_3 aggregates increased with increasing the nano-ZrO_2 content.

The specific surface area (S_g) of Al_2O_3, Y-PSZ, Al-doped Y-PSZ, 10.5ZN and 22ZN powders was 8.74, 7.84, 12.25, 9.7 and 13 m^2/g, respectively. Fig. 3a–c shows SEM micrographs of Al_2O_3, Y-PSZ and Al-doped Y-PSZ, respectively. The shape of Al-doped Y-PSZ particles was different with respect to that of Al_2O_3 and Y-PSZ; Al_2O_3

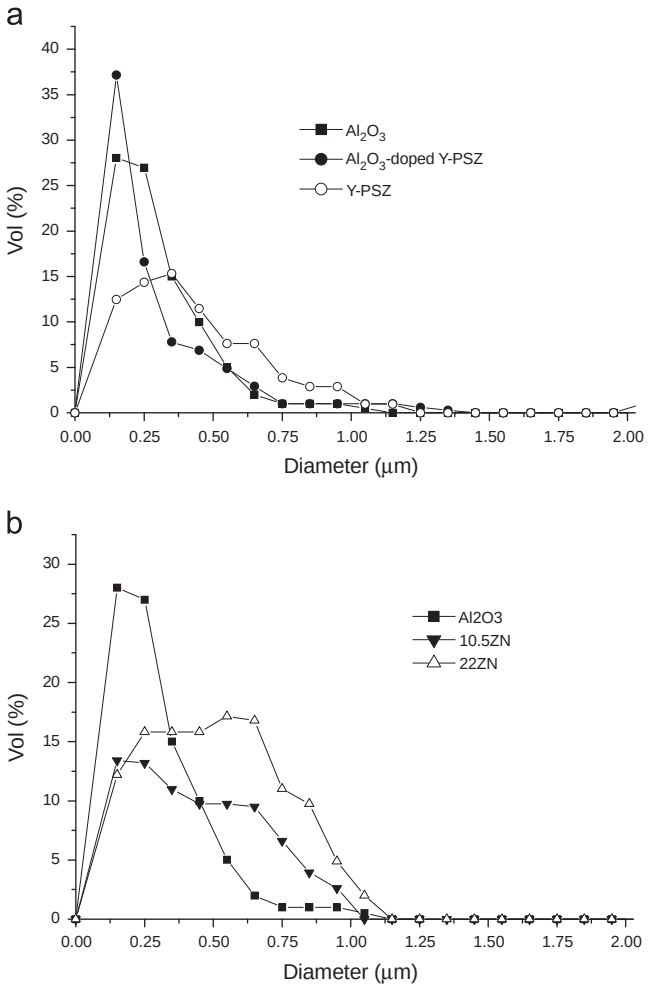

Fig. 2. Particle size distribution curves of different powders: (a) Al_2O_3, Y-PSZ and Al-doped Y-PSZ and (b) Al_2O_3, 10.5 and 22ZN powders after milling.

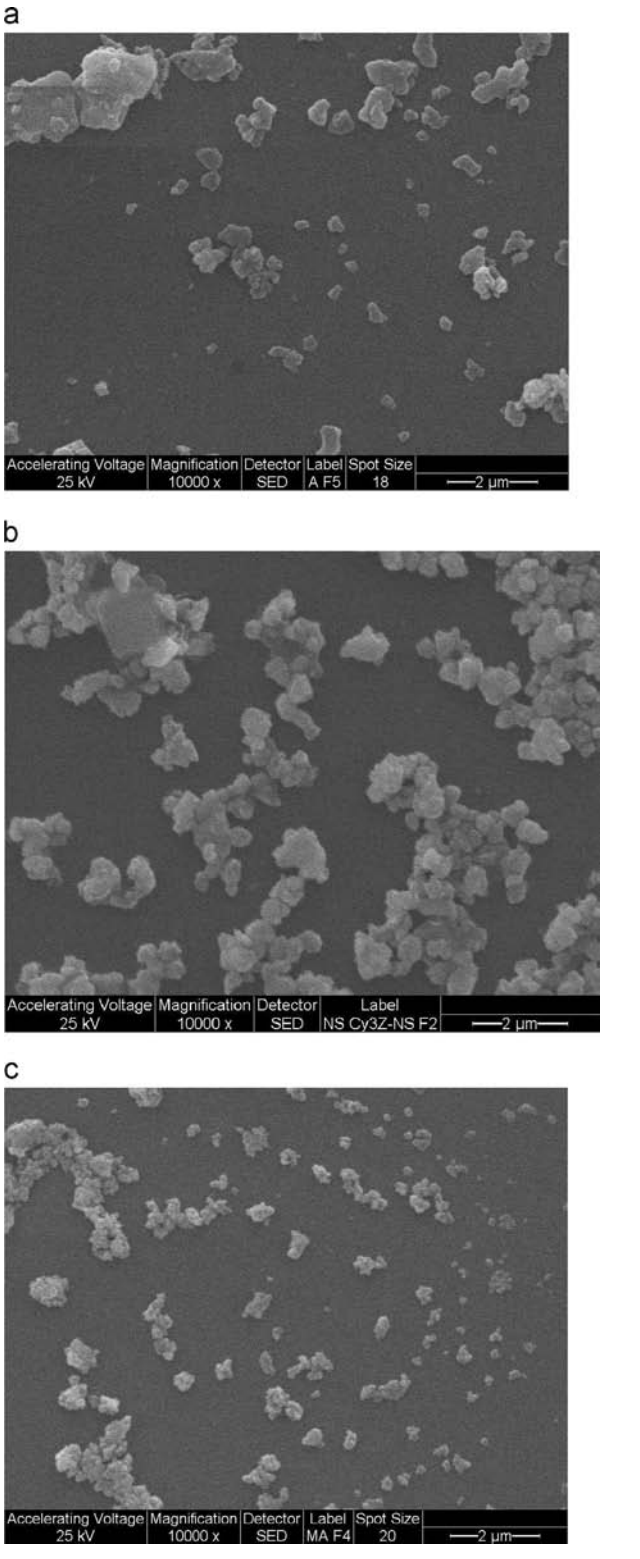

Fig. 3. SEM micrographs of different powders: (a) Al_2O_3, (b) Y-PSZ, and (c) Al-doped Y-PSZ.

and Y-PSZ particles showed smooth and sharp edges while Al-doped Y-PSZ presented round and rough ones; this last shape contributed to an increase in the S_g of Al-doped Y-PSZ powder. As we have mentioned Al-doped Y-PSZ powder contained 0.3 wt% Al_2O_3, phase equilibrium studies have shown that Al_2O_3 and ZrO_2 are compatible [9]; Al_2O_3 does not form solid solution with zirconia due to its low solubility therefore a surface coating of Al_2O_3 on ZrO_2 is expected. The finer particles, the particle shape and the surface coating of Al-doped Y-PSZ were responsible to its higher specific surface area with respect to that of Al_2O_3 and Y-PSZ. In Fig. 4 the SEM micrographs of 10.5 and 22 ZN were compared. The shape of ZN particles was similar to that of Al_2O_3 (Figs. 3a and 4); greater particle sizes with respect to those of Al_2O_3 were found for the 22ZN, due to aggregation; less aggregation of Al_2O_3 particles was observed for the10.5ZN, these observations were in accordance with the particle size distribution measurements. The higher S_g of the ZN powders with respect to that of Al_2O_3 could be attributed to the nano-sized ZrO_2 coating on the Al_2O_3 particles.

Fig. 5 shows the zeta potential vs. pH curves of the different powders. The IEP of Al-doped Y-PSZ, Al_2O_3, Y-PSZ, 10.5 and 22ZN powders was found to be 8.9, 8.5, 7, 6 and 4.3, respectively. The Al_2O_3 and Y-PSZ IEPS were in

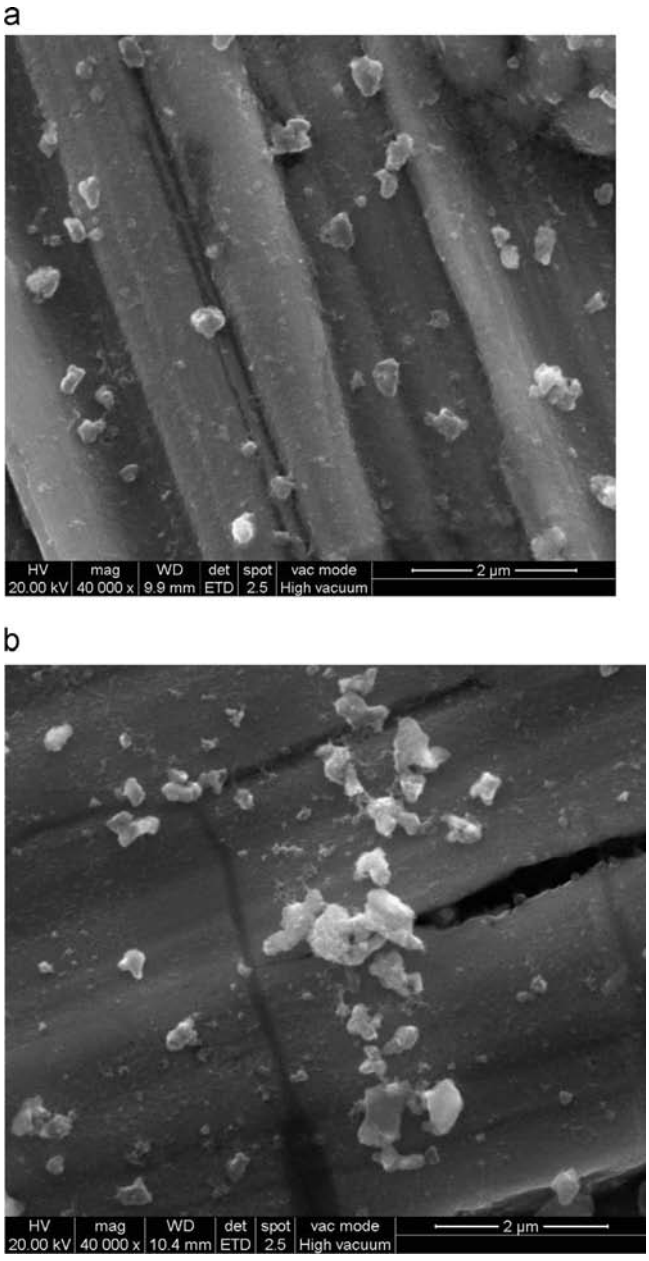

Fig. 4. SEM micrographs of different powders: (a) 10.5 ZN and (b) 22ZN.

agreement with those reported in the literature for these powders [2,10]; however, the IEP of Al-doped Y-PSZ powder was close to that of Al_2O_3 and higher than that of Y-PSZ. Thus, the Al_2O_3 surface coating shifted the pH_{IEP} of Y-PSZ from 7 to 8.9. The surface charge properties of the Al-doped Y-PSZ particles changed from Y-PSZ-like to Al_2O_3-like. On the contrary, the very fine zirconia particles homogeneously distributed on the Al_2O_3 particles surface shifted the pH_{IEP} of Al_2O_3 from 8.5 to 6 for 10.5ZN and from 8.5 to 4.3 for 22ZN. The pH_{IEP} decreased with increasing the ZN content and for 22ZN the pH_{IEP} became similar to that reported for ZrO_2 which was about 4–6 [11,12]. The magnitude of the negative zeta potential at pH 9 was −0.77, −13, −35, −40 and −57.5 mV for Al-doped Y-PSZ, Al_2O_3,Y-PSZ, 10.5 and 22ZN powders, respectively.

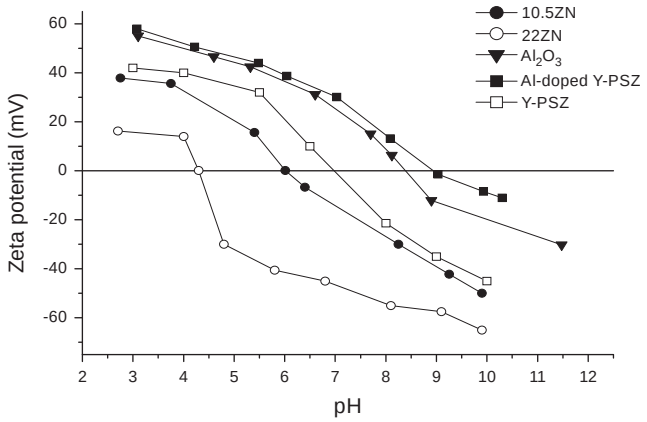

Fig. 5. Zeta potential vs. pH curves of different powders: Al_2O_3, Y-PSZ, Al-doped Y-PSZ, 10.5 and 22ZN.

Fig. 6 shows the mean particle diameter (d_{50}) as a function of pH for Al_2O_3, Y-PSZ, Al-doped Y-PSZ, 10.5 and 22ZN powders. Al_2O_3 could be dispersed at pH values < 6.5; the d_{50} increased with increasing pH from 6.5 to 7.5, then it remained nearly constant with further increasing in pH. In the pH range from 3 to 6 the particles became well dispersed indicating an increase in the electrostatic repulsion between particles. At pH > 6 a reduction in the electrostatic repulsion between particles was expected due to the strong flocculation; the Van der Waals attraction forces were dominant and caused aggregation of the particles. This aggregation still remained up to pH 9.6 indicating a low negative surface charge of the Al_2O_3 powder in that basic pH region.

The aqueous dispersion of Al-doped Y-PSZ was similar to that of Al_2O_3; Al-doped Y-PSZ powder could be dispersed at pH values < 6.5; aggregation between particles occurred in the pH range 7.5–9.6. The aqueous dispersion of Y-PSZ was similar to that of Al-doped Y-PSZ up to pH 8.1, at pH values > 8.1 the Y-PSZ particles became well dispersed indicating an increase in the electrostatic repulsion between particles. The Y-PSZ powder could be dispersed at pH 9, this behavior was markedly different from that observed for Al_2O_3 and Al-doped Y-PSZ powders. Thus, the magnitude of the negative surface charge of Y-PSZ at pH 9 was high enough to impart stability to the suspensions.

The d_{50} vs. pH curves were consistent with the zeta potential measurements (Fig. 5): (1) Al_2O_3 and Al-doped Y-PSZ powders could be dispersed at pH < 6.5 while Y-PSZ powder at pH < 5.5 due to their high positive zeta potential, (2) the magnitude of Al_2O_3 and Al-doped Y-PSZ powders zeta potential in the pH region 7.5–9.6 was not high enough to stabilize the suspensions, and (3) the higher negative zeta potential of Y-PSZ at pH 9 with respect to that of Al_2O_3 and Al-doped Y-PSZ produce a well dispersed suspension.

10.5ZN powder could be dispersed at pH values < 5; aggregation between particles occurred in the pH range 6–7.2, and at pH values > 7.2 the particles became well-dispersed. For the 22ZN powder a strong flocculation was found at about pH 4 causing aggregation of the particles, this aggregation still remained up to pH 7.5. The magnitude of the

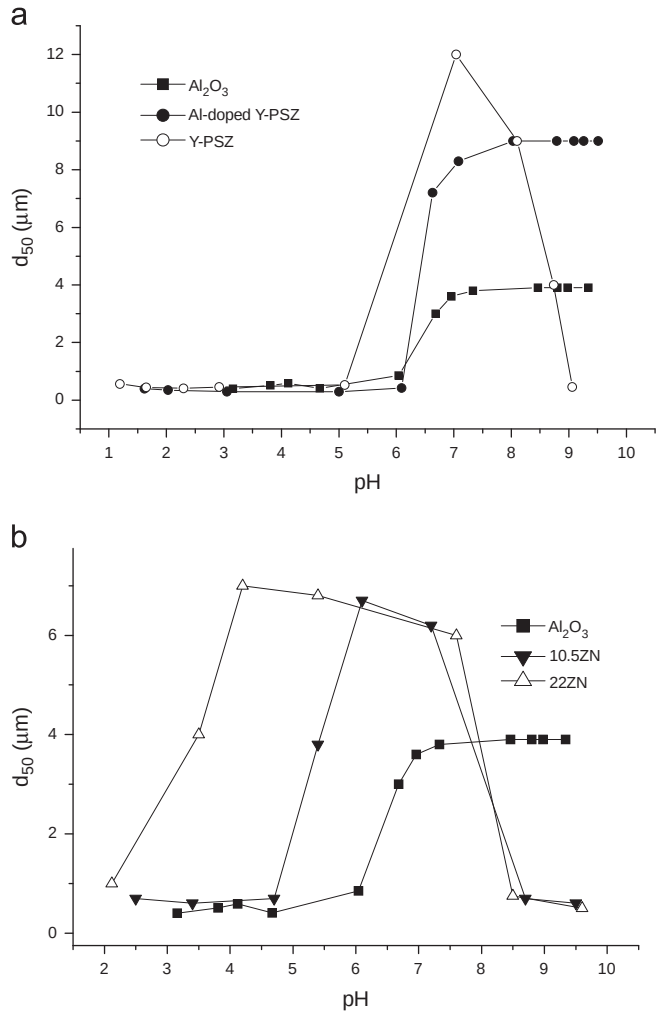

Fig. 6. Mean particle diameter (d_{50}) as a function of pH for different powders. (a) Al_2O_3, Y-PSZ and Al-doped Y-PSZ, and (b) Al_2O_3, 10.5 and 22 ZN powders.

Table 2
Optimum NH_4PA concentration for the different compositions of Al_2O_3–ZrO_2 suspensions at pH 9.

Slurry composition	Optimum NH_4PA concentration (wt%)[a]	Slurry viscosity (mPa s at $\gamma = 542\ s^{-1}$)
10.5Al-doped Y-PSZ	0.34	8.1
10.5Y-PSZ	0.25	6.6
10.5ZN	0.30	11.0
22Al-doped Y-PSZ	0.40	9.0
22Y-PSZ	0.21	6.7
22ZN	0.40	11.7
50Al-doped Y-PSZ	0.52	12.5
50Y-PSZ	0.11	4.0

[a]Dry weight basis of powder.

negative zeta potential of 22ZN at pH 7–7.5 was high enough to stabilize the suspension, however, aggregation of particles was found at that pH range. Thus, for this powder the d_{50} vs. pH curve was not in agreement with its zeta potential curve. This behavior was also found by Fengqiu et al. [12] who studied the dispersion properties of nano-zirconia suspensions. They explained that under slightly basic conditions the OH^- adsorbed on the few positive sites of the 22 ZN particle surface could bond with a negative site of another particle by hydrogen bond. Thus, the hydrogen bonds between the 22ZN particles seemed to be responsible for the particles aggregation at pH 7–7.5. At pH >8 the positive sites on the 22ZN particles markedly decreased and consequently the OH^- adsorption, thereby the hydrogen bonds could not be established and the particles became well-dispersed.

3.2. Optimum NH_4PA concentration, amount of NH_4PA adsorbed and zeta potential for the different compositions.

The optimum NH_4PA concentration, i.e. which gave slips with the lowest viscosity, was determined by measuring the viscosity of 35 vol% slips at a shear rate (γ) of 542 s^{-1} as a function of the amount of NH_4PA solution added at pH 9 for the slips with the different compositions. These results are presented in Table 2. The optimum NH_4PA concentration decreased from 0.34 to 0.25, 0.4 to 0.21 and 0.52 to 0.11 wt% by substituting 10.5, 22 and 50 vol% of Al-doped Y-PSZ by Y-PSZ in the mixtures, respectively. The minimum viscosity occurred at 0.3 and 0.4 wt% NH_4PA solution for the 10.5 and 22ZN powders, respectively. For the mixtures with the same composition, the viscosity values were lower for the slips prepared with Y-PSZ; whereas, the ZN slips exhibited the highest viscosity values.

Fig. 7 shows the amount of NH_4PA adsorbed for 35 vol% slips with the optimum NH_4PA concentration at pH 9 as a function of zirconia content in the mixtures. The adsorption of the polyelectrolyte increased from 0.20 to 0.33 mg/m^2 with increasing Al-doped Y-PSZ concentration from 0 to 50 vol%, respectively. As previously shown in the zeta potential curves (Fig. 5), the substitution of Al_2O_3 by Al-doped Y-PSZ in the mixtures decreased the magnitude of the negative zeta potential at pH 9, consequently a high adsorption of the anionic polymer was expected. The electrostatic repulsion between the negatively charged powders and the anionic polymer decreased with increasing Al-doped Y-PSZ content, thereby increasing the amount of NH_4PA adsorbed. On the contrary, the polymer adsorption decreased with increasing the Y-PSZ content in the mixtures; this could be attributed to the increase in the magnitude of the negative zeta potential by substituting Al_2O_3 for Y-PSZ in the mixtures (Fig. 5). The NH_4PA adsorption on the ZN powders also decreased with increasing the ZN content and a lower adsorption of ZN powders with respect to that of the conventional mixtures was found due to their higher negative zeta potential values at pH 9 (Fig. 5).

The adsorption behavior of the Al_2O_3–ZrO_2 mixtures at pH 9 is not of "high-affinity type" [13]; the electrostatic repulsion at the surface imparts a barrier for adsorption which limits adsorption to low amounts [8]. However, the

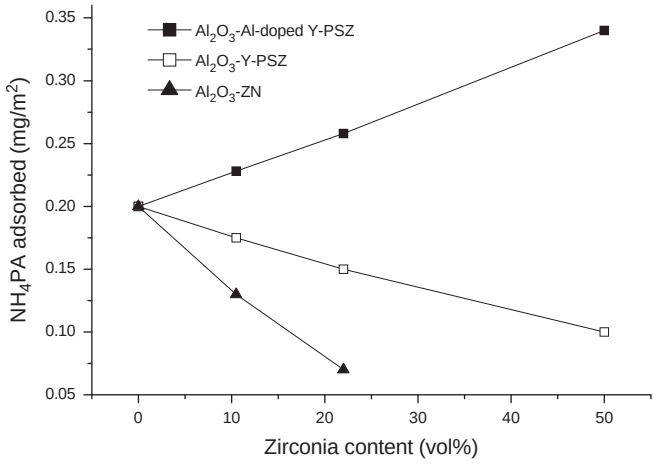

Fig. 7. Amount of NH_4PA adsorbed for 35 vol% slips with the optimum NH_4PA concentration as a function of zirconia content in the mixtures.

fact that adsorption occurred under these conditions indicated that there was a "specific" or "chemical" segment–surface interaction which overcompensated the repulsive electrostatic forces. Previous studies on alumina [14] and coated silicon nitride [15], also found a detectable adsorption of anionic polyelectrolytes when the polyelectrolyte and the surface had the same charge sign. For the compositions with the same zirconia content, the NH_4PA adsorption was higher for Al-doped Y-PSZ compared with that of Y-PSZ and ZN; this adsorption difference tended to be more pronounced with increasing zirconia content.

Fig. 8a shows the zeta potential vs. pH curves of different powders: Al_2O_3, 22Al-doped Y-PSZ and 22Y-PSZ dispersed in slips with the optimum amount of NH_4PA solution added. In Fig. 8b the zeta potential vs. pH curves of the ZN powders in suspensions with the optimum amount of NH_4PA solution added are compared with that of Al_2O_3. The adsorption of NH_4PA shifted the pH_{IEP} of Al_2O_3 (Fig. 5) from pH 8.5 to 3.1; the IEP of the mixtures 22Y-PSZ and 22Al-doped Y-PSZ was found to be 4.25 and lower than 3, respectively. The strong adsorption of the polyelectrolyte on the mixture 22Al-doped Y-PSZ (Fig. 7) resulted in an increase in the magnitude of the negative zeta potential in the pH range 3.25–10.1. The higher pH_{IEP} of the mixture 22Y-PSZ with respect to that of 22Al-doped Y-PSZ and Al_2O_3 was a consequence of the lower adsorption of the polyelectrolyte (Fig. 7). The zeta potential value at pH 9 was −45.5, −57.3 and −62.7 mV for Al_2O_3, 22Y-PSZ and 22Al-doped Y-PSZ, respectively.

The IEP of 10.5 and 22ZN was found to be 3.4 and 2.2, respectively (Fig. 8b). The lower adsorption of the ZN powders with respect to that of Al_2O_3 (Fig. 7) produced a lesser displacement of their pH_{IEPs} (Fig. 5). Similar negative zeta potential values of the 22ZN slips with and without NH_4PA at alkaline pH were observed as a consequence of the very low adsorption of the polyelectrolyte Figs. 5, 7 and 8b). The zeta potential value at pH 9 was −45.5, −52.5 and −57.5 mV for Al_2O_3, 10.5 ZN and

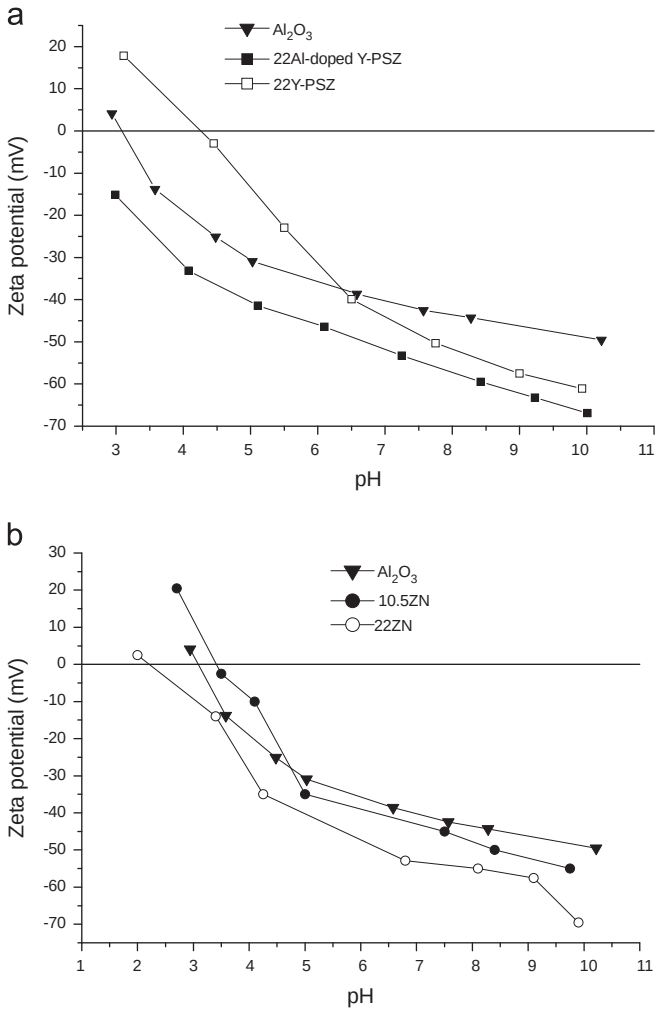

Fig. 8. Zeta potential vs. pH curves of different powders dispersed in slips with the optimum amount of NH_4PA solution added: (a) Al_2O_3, 22Al-doped Y-PSZ and 22Y-PSZ, and (b) Al_2O_3, 10.5ZN and 22ZN.

22 ZN slips with the optimum amount of NH_4PA solution added, respectively. The high adsorption of the negatively charged polyelectrolyte on Al_2O_3 produced a significantly increase in its negative surface charge at pH 9. On the contrary, the high negative zeta potential of the ZN powders at pH 9 (Fig. 5) mainly contributed to their negative surface charge with NH_4PA since the NH_4PA adsorption was very low. The negative zeta potential at pH 9 for 22Y-PSZ and 22Al-doped Y-PSZ slips with the optimum amount of NH_4PA solution added was similar to that of ZN slips and high enough to impart stability to the suspensions.

At pH 9 the suspensions with the optimum NH_4PA concentration were dominated by repulsive forces, thus, they were stabilized. The adsorption of the negatively charged polyelectrolyte enhanced the negative surface charge of the powders. In addition, at pH 9 the electrostatic repulsion between the charged carboxylate groups prevents the accumulation of groups at the surface, the polyelectrolyte adsorbs in a stretched-out configuration

which results in long-range steric interactions of the NH_4PA at the solid–liquid interface [13]. Thus, the adsorbed molecules increased the electrosteric repulsion between particles, consequently the slip viscosity attained the minimum value (Table 2).

3.3. Rheological properties

Fig. 9a shows the viscosity at 542 s^{-1} vs. the zirconia content for stabilized slips at pH 9 with different solid loading. The measured flow curves were satisfactorily fitted with the Casson model (R=0.99). The Casson model equation is

$$\tau^{1/2} = \tau_0{}^{1/2} + (\eta_p \gamma)^{1/2} \quad (1)$$

where τ is the shear stress, γ is the shear rate, τ_0 is the yield stress and η_p represents the limiting viscosity at a high shear rate range. The particles in a flocculated suspension form floc groups or a network because of the mutual attraction between particles; the aggregated particles make the suspension difficult to flow, thereby increasing the τ_0 value [8]. Consequently, the τ_0 value of the Casson model could be used as a parameter that indicated the degree of aggregation and consequently the degree of slip flocculation. The effect of zirconia content on the τ_0 value for different solid loading is shown in Fig. 9b.

For Al_2O_3–ZN and Al_2O_3–Al-doped Y-PSZ slips, the viscosity and τ_0 values increased with increasing the zirconia content in the mixtures; while for Al_2O_3–Y-PSZ slips, a decrease in the viscosity and τ_0 with increasing Y-PSZ content were found. For all the concentrations, the τ_0 values of Al_2O_3–ZN slips were markedly higher than those of Al_2O_3–Al-doped Y-PSZ and Al_2O_3–Y-PSZ ones; these differences became larger as the zirconia content increased. The τ_0 values of 48 vol% slips prepared from 22ZN, 22 Al-doped Y-PSZ and 22Y-PSZ decreased from 6.5 to 2.2 and 1.1 Pa, respectively. The important resistance to flow for the Al_2O_3–ZN slips was attributed to the presence of some aggregated particles. As the degree of aggregation increased with increasing ZN content, the difference in the τ_0 values between the Al_2O_3–ZN slips and those prepared from the different zirconia powders tended to be more pronounced with increasing zirconia content. Besides, an important increase in the slopes of the τ_0 curves with increasing solid loading were found for the different slips. As the solid content increases particles are forced to approach each other and overlap their electrical double layers (electroviscous effect), as the repulsion between particles decreases the number of flocs increases, as well as the quantity of entrapped liquid not available for flow [16]. The increase in the yield stress with increasing solid loading was attributed to a higher frequency of the collisions between separate particles, increasing the resistance to flow. Therefore, the difference in the τ_0 values between the different slips became larger with increasing both the zirconia content and the solid loading. The degree of aggregation of the 10.5 and 22ZN particles had more

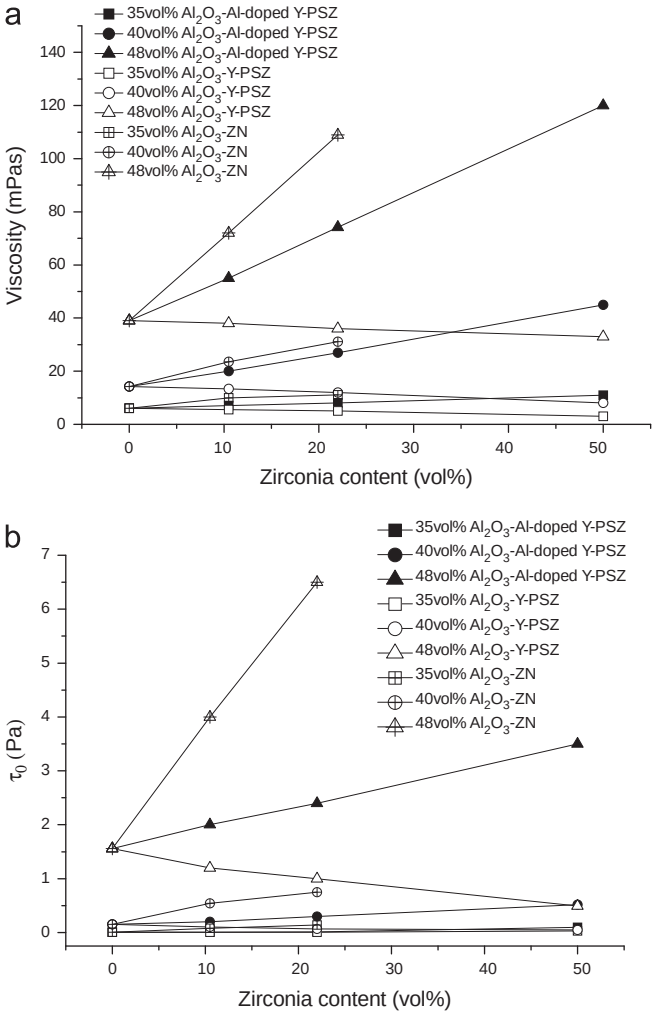

Fig. 9. Viscosity at 542 s^{-1} (a) and τ_0 (b) vs. the zirconia content for stabilized Al_2O_3–Y-PSZ, Al_2O_3–Al-doped Y-PSZ and Al_2O_3–ZN slips at pH 9 with different solid loading.

effect on the τ_0 than on the viscosity values "as expected". Since the negative zeta potential of the ZN slips were high, the high viscosity values of these slips could be attributed to the presence of some aggregated particles which increased the quantity of entrapped liquid not available for flow.

A significant increase in the viscosity values of Al_2O_3–Al-doped Y-PSZ slips with respect to Al_2O_3–Y-PSZ ones was found for all the compositions and solid loading studied (Fig. 9a). As previously shown (Fig. 8a) the negative zeta potential at pH 9 for the slips with the same content of Y-PSZ and Al-doped Y-PSZ were similar and high enough to impart stability to the suspensions. The higher viscosity values of the suspensions prepared from Al-doped Y-PSZ could be explained taking into account the particle effective size concept. The calculated volume fraction of solids corresponded to the solid loading of the slurries and did not consider hydrated and adsorbed layers around the particles. The distinction between size and effective size of the particles becomes important when high

solid loading and/or particles with high specific surface area are used [16].

Table 3 lists the values of the maximum packing fraction (ϕ_m) for different 48 vol% slips: Al_2O_3, 50Al-doped Y-PSZ and 50Y-PSZ with the optimum amount of NH_4PA solution added. ϕ_m increased with decreasing the volume of solid sediment. Similar ϕ_m values were found for Al_2O_3 and 50Y-PSZ suspensions; however, significantly lower ϕ_m values were observed for 50Al-doped Y-PSZ slips. This indicated that higher volumes of solid sediment were measured when the same content of Al_2O_3 or Y-PSZ was substituted by Al-doped Y-PSZ, resulting in a reduction of the maximum particle packing. Consequently, the effective size of the Al-doped Y-PSZ particles could be assumed to be larger than that of both Al_2O_3 and Y-PSZ. Since the specific surface area of the Al-doped Y-PSZ particles was markedly higher than that of Al_2O_3 and Y-PSZ, a greater hydration surrounding the Al-doped Y-PSZ particles was expected. Besides, the substitution of Al_2O_3 and/or Y-PSZ by Al-doped Y-PSZ increased the polymer adsorption (Fig. 5). Therefore, the substitution of Al_2O_3 and/or Y-PSZ by Al-doped Y-PSZ in the mixtures increased the effective solid volume fraction at a given solid loading and decreased the amount of free-liquid available for flow, thereby increasing the viscosity values. The differences in the viscosity values tended to be more pronounced with increasing both the Al-doped Y-PSZ content and the solid loading, confirming the hypothesis regarding the higher effective solid volume fraction of the Al-doped Y-PSZ particles.

Table 3
Maximum packing fraction (ϕ_m) for different 48 vol% slips with the optimum amount of NH_4PA solution added.

Slurry composition	ϕ_m (%)
Al_2O_3	54.4
50Y-PSZ	55.8
50Al-doped Y-PSZ	48

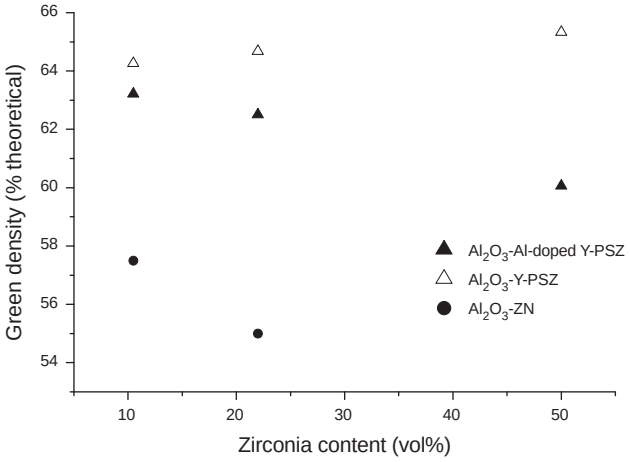

Fig. 10. Green density of cast samples prepared from 48 vol% Al_2O_3 –Y-PSZ, Al_2O_3–Al-doped Y-PSZ and Al_2O_3–ZN slips vs. the zirconia content in the mixtures.

3.4. Characterization of green and sintered samples

Fig. 10 shows the green density of cast samples prepared from 48 vol% Al_2O_3–Y-PSZ, Al_2O_3–Al-doped Y-PSZ and Al_2O_3–ZN slips vs. zirconia content. The green density curves for Al_2O_3–ZrO_2 bodies were opposite to those of the viscosity vs. zirconia content (Fig. 9a), as the slip viscosity decreased a more dense packing of the samples could be obtained. The better slip dispersion of the Al_2O_3–Y-PSZ slips resulted in higher green density values for all the compositions. The difference in the green density values became greater as the zirconia content increased in accordance with the viscosity and yield stress results.

In the stable suspensions, the particles could pack in an ordered way, due to the repulsive forces existing between them; the low deposition rate also enabled each particle to search for energetically favorable positions. In this condition, dense packing of particles could be obtained. As the slip viscosity increased the mutual approach of the particles increased; hence, the searching of one particle for a low energy position was disturbed and hindered to achieve an optimum particle packing. Consequently, a less dense particle packing with increasing the slip viscosity could be expected. For Al_2O_3–Y-PSZ slips, green density values between 64.3% (10.5Y-PSZ) and 65.3% (50Y-PSZ) of theoretical density were found; while for Al_2O_3–Al-doped Y-PSZ slips, the green density had values between 63.2% (10.5Al-doped Y-PSZ) and 60.0% (50Al-doped Y-PSZ) of theoretical density. Thus, the substitution of Y-PSZ by Al-doped Y-PSZ in the Al_2O_3–ZrO_2 mixtures increased the slip viscosity with NH_4PA resulting in a less dense packing of cast samples. The cast samples obtained from the Al_2O_3–ZN slips exhibited the lowest green density values: 57.0% and 54.0% of the theoretical density for 10.5 and 22ZN, respectively.

The sintered density of the composites with 10.5 vol% ZrO_2 was compared. The sintered density values were 97.3, 97.8 and 97.7% of the theoretical density for 10.5ZN, 10.5Al-dopedY-PSZ and 10.5Y-PSZ, respectively. Although the green density of the 10.5ZN was markedly lower than that of 10.5Al-dopedY-PSZ and 10.5Y-PSZ (Fig. 10), the sintered density of the 10.5ZN was as high as the others composites. The fine ZrO_2 particles homogeneously distributed on the Al_2O_3 particle surfaces increased the densification rate and a high sintered density could be achieved.

Fig. 11 shows the final microstructure of the different bodies with 10.5 vol% ZrO_2 sintered at 1600 °C, and Fig. 12 shows the zirconia grain size distribution curves obtained for the different composites. ZrO_2 grains homogeneously distributed, avoiding agglomerates, at the alumina grain boundaries were observed for 10.5ZN. The zirconia grain size distribution curves for 10.5Al-doped Y-PSZ and 10.5Y-PSZ were similar. The 10.5Al-doped Y-PSZ curve was slightly shifted to lower grain diameters

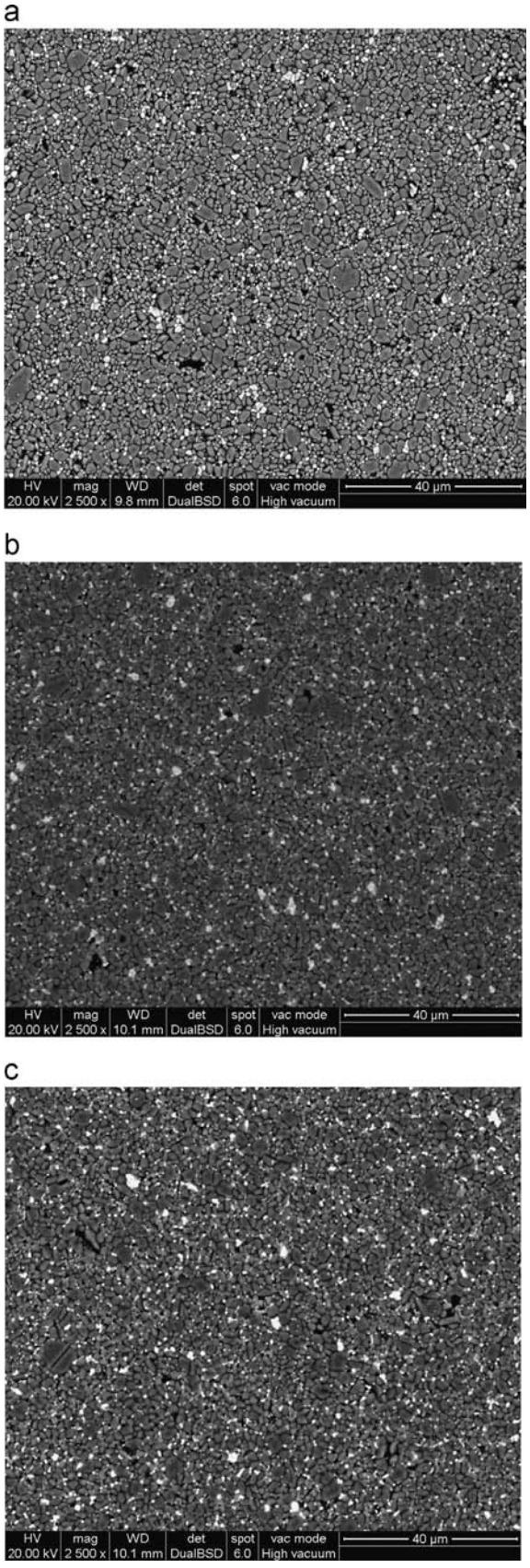

Fig. 11. Microstructure of the different bodies with 10.5 vol% ZrO_2 sintered at 1600 °C. ZrO_2 grains (the brighter phase) homogeneously distributed in a fine grain Al_2O_3 matrix (the darker phase). (a) 10.5ZN, (b) 10.5Al-doped Y-PSZ, and (c) 10.5Y-PSZ.

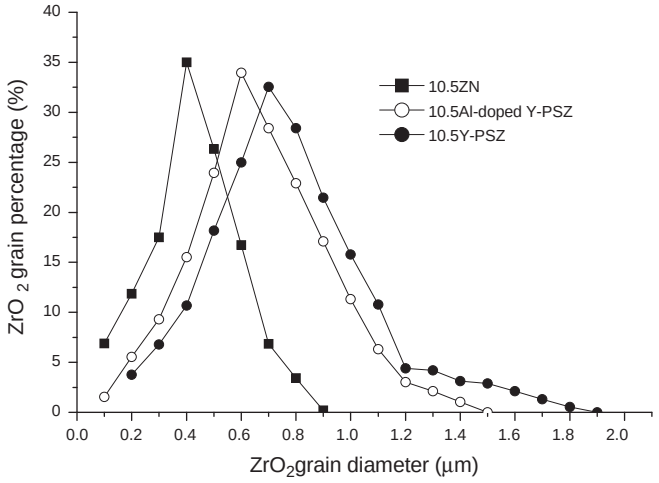

Fig. 12. Zirconia grain size distribution curves obtained for the different composites with10.5 vol% ZrO_2 sintered at 1600 °C.

with respect to the 10.5Y-PSZ curve; the more frequent grain diameters were 0.6 and 0.7 µm for 10.5Al-doped Y-PSZ and 10.5Y-PSZ, respectively.

The Zr (IV) precursor route let to a narrower and smaller zirconia grain size distribution compared with the conventional powder mixing route. The ZrO_2 grain diameters were in the range 0.1–0.8 µm and the more frequent grain diameter was 0.4 µm. Thus, almost all the ZrO_2 grains could be kept below the critical size for spontaneous transformation after sintering. These particles were also greater than the critical size for transformation during crack growth. Therefore, it would be possible to retain a larger amount of tetragonal zirconia grains in the alumina matrix and this would contribute to the transformation toughening mechanism operating in these composites.

4. Conclusions

Two Al_2O_3–ZrO_2 mixture preparation routes: classical powder mixing and addition of a Zr (IV) precursor solution to a well dispersed Al_2O_3 suspension, were used to produce Al_2O_3–ZrO_2 slip cast composites. For the conventional powder mixing route, two commercial 3 mol% yttria-partially stabilized zirconia powders, 0.3 wt% Al_2O_3-doped (Al-doped Y-PSZ) and without Al_2O_3 (Y-PSZ), were employed. The rheological properties of Al_2O_3–ZrO_2 suspensions prepared with the different zirconia powders and the Zr (IV) precursor, and their particle packing behavior during slip casting were compared. The viscosity and yield stress values of Al_2O_3–ZN slips were markedly higher than those of Al_2O_3–Al-doped Y-PSZ and Al_2O_3–Y-PSZ ones; these differences became larger with increasing both the zirconia content and the solid loading. The high resistance to flow for the Al_2O_3–ZN slips was attributed to the presence of some aggregated particles; the degree of aggregation increased with increasing ZN content from 10.5 to 22 vol%. The cast samples obtained from the Al_2O_3–ZN slips exhibited the lowest green density values; however,

for 10.5ZN a high sintered density and a smaller zirconia grain size distribution could be achieved. The small ZrO_2 grains would lead to a high portion of tetragonal phase retained in the alumina matrix after sintering with the ability to transform under applied stress.

References

[1] J. Wang, R. Stevens, Review zirconia–toughened alumina (ZTA) ceramics, Journal of Materials Science 24 (10) (1989) 3421–3440.

[2] S. Olhero, I. Ganesh, P. Torres, F. Alves, J.M.F. Ferreira, Aqueous colloidal processing of ZTA composites, Journal of the American Ceramic Society 92 (1) (2009) 9–16.

[3] C. Piconi, G. Maccauro, Zirconia as a biomaterial, Biomaterials 20 (1999) 1–25.

[4] Y. Shin, Y. Rhee, S. Kang, Experimental evaluation of toughening mechanism in alumina-zirconia composites, Journal of the American Ceramic Society 82 (5) (1999) 1229–1232.

[5] H.J. Hannink, P.M Kelly, B.C. Muddle, Transformation toughening in zirconia-containing ceramics, Journal of the American Ceramic Society 83 (3) (2000) 461–487.

[6] A.H. De Aza, J Chevalier, G. Fantozzi, M. Schehl, R. Torrecillas, Crack growth resistance of alumina, zirconia and zirconia toughened alumina ceramics for joint prostheses, Biomaterials 23 (2002) 937–945.

[7] J. Cesarano III, I.A. Aksay, A. Bleier, Stability of aqueous α-alumina suspensions with poly(methacrylic acid) polyelectrolyte, Journal of the American Ceramic Society 71 (4) (1988) 250–255.

[8] H. Guldberg-Pedersen, L Bergstrom, Stabilizing ceramic suspensions using anionic polyelectrolytes: adsorption kinetics and interparticle forces, Acta Materials 48 (1988) 4563–4570.

[9] F.F. Lange, D.J. Green, Effect of inclusion size on the retention of tetragonal ZrO_2:theory and experiments, Advances in Ceramics, Science and Technology of Zirconia 3 (1981) 222–223.

[10] M.P. Albano, L.B. Garrido, Improvement in the colloidal processing of concentrated silicon nitride slips with ammonium polyacrylate by an yttria-alumina surface coating, Colloids and Surfaces A 248 (2004) 1–8.

[11] S. Prakash Rao, S.S. Tripathy, A.M. Raichur, Dispersion studies of sub-micron zirconia using Dolapix CE 64, Colloids and Surfaces A 302 (2007) 553–558.

[12] T. Fengqiu, H. Xiaoxian, Z. Yufing, G. Jingkun, Effect of dispersant on surface chemical properties of nano-zirconia suspensions, Ceramics International 26 (2000) 93–97.

[13] D. Liu, S.G. Malgham, Role of polyacrylate in modifying interfacial properties and stability of silicon nitride particles in aqueous suspensions, Colloids Surface A 110 (1996) 37–45.

[14] J. CesaranoIII, I.A. Aksay, Processing of highly concentrated aqueous α-alumina suspensions stabilized with polyelectrolytes, Journal of the American Ceramic Society 71 (12) (1988) 1062–1067.

[15] M.P. Albano, L.B Garrido, A.B. Garcia, Dispersion of aluminium hydroxide coated Si_3N_4 powders with ammonium polyacrylate dispersant, Colloids Surface A 181 (2001) 69–78.

[16] G. Tari, M.F. Ferreira, and Lyckfeldt. Influence of the stabilising mechanism and solid loading on slip casting of alumina, Journal of the European Ceramic Society 18 (1998) 479–486.